10.1109/ULTSYM.2009.0076

Implementation of Scatterer Size Imaging on an Ultrasonic Breast Tomography Scanner

Roberto J. Lavarello and Michael L. Oelze
Bioacoustics Research Laboratory
Department of Electrical and Computer Engineering
University of Illinois at Urbana-Champaign
Urbana, IL 61801
Email: lavarell@illinois.edu

Michael Berggren and Steven Johnson
TechniScan, Inc.
3216 Highland Drive suite 200
Salt Lake City, UT 84106

Marko Orescanin
Department of Electrical and Computer Engineering
University of Illinois at Urbana-Champaign
Urbana, IL 61801

Rebecca Yapp
Department of Bioengineering
University of Illinois at Urbana-Champaign
Urbana, IL 61801

***Abstract*—Quantitative ultrasound (QUS) techniques make use of frequency-dependent information from backscattered echoes normally discarded in conventional B-mode imaging. Using scattering models and spectral fit methods, properties of tissue microstructure can be estimated. The use of full angular spatial compounding has been proposed as a means of improving the variance of scatterer property estimates and spatial resolution of QUS imaging. In this work, preliminary experimental results from a QUS implementation on an ultrasonic breast tomography scanner from TechniScan, Inc. are presented. The imaging target consisted of a cylindrical gelatin phantom of 7.8 cm diameter. The phantom contained uniformly distributed glass bead inclusions of 85 m mean diameter. The scanner provided reflection-mode data using arrays with 6 MHz nominal center frequency for 17 different angles of view distributed between 0° and 360°. Tomographic images of speed of sound were also generated by the scanner and used for refraction-compensation and registration of the effective scatterer diameter (ESD) estimates corresponding to ROIs at different angles of view. Only data from the surface of the array to the center of the tomography gantry were analyzed for each angle of view, which resulted in 8.5 effective angles of view per ROI. ESD estimates were obtained using ROIs of size 4 mm by 4 mm with a 50% overlap. The average mean and standard deviation of the single angle of view estimates considering the 17 data sets were 85.4 μm and 12.2 μm, respectively. The resulting ESD mean and standard deviation of the compounded image were 85.2 μm and 4.1 μm, respectively. The preliminary experimental results presented here represent the first implementation of QUS on an ultrasonic breast tomography scanner and demonstrate some of the benefits of integrating these technologies, i.e., the availability of full angular spatial compounding and integration with tomographic speed of sound images.**

I. Introduction

The quantitative ultrasound (QUS) imaging technique based on ultrasonic backscatter has proven potential for animal and human tissue characterization [1]–[5]. Previously, the use of limited [6], [7] and full [8] angular spatial compounding has been shown to extend the trade-off between spatial resolution and variance in the estimates. In particular, and based on the results presented in [8], it is hypothesized here that QUS imaging can achieve an improved performance on tomographic devices capable of producing views of an object from 360°. In order to experimentally validate this assertion, QUS was implemented on the Whole Breast Ultrasound (WBU) scanner by Techniscan, Inc. [9].

II. Methods

A. QUS estimation

QUS estimates were calculated from measurements of backscattering coefficients, which can be obtained at different depths for each scan line by calculating the magnitude of the power spectrum of the radiofrequency (rf) data after gating with a windowing function. The following formulation assumes that no multiple scattering was produced in the insonified medium and that speed of sound and density variations were only a small percentage of the background value. Neglecting attenuation and assumming plane wave illumination, the backscattered pressure $P_m(f)$ produced by a random distribution of N identical scatterers randomly distributed in a fluid media can be expressed as

$$p_m(t) = p_0(t) * \sum_{i=1}^{N} g(t - t_i, \mathrm{ESD}), \tag{1}$$

where $p_0(t)$ is the transmit-receive impulse response of the transducer, $g(t)$ is the scattering function of a single scatterer, t_i is the time of arrival of the signal due to the i-th scatterer, and the $*$ symbol represents the convolution operation. The property of interest in this study is the effective scatterer diameter (ESD), which represents the typical size of unresolvable scatterers within the insonified region. In frequency domain, the backscattered intensity can be expressed as

$$S_m(f) = S_0(f)S_g(f,\text{ESD})\left\{N + 2\sum_{i>j}^{N}\cos\left(2\pi f[t_i - t_j]\right)\right\}, \quad (2)$$

where $S_0(f)$ and $S_g(f,\text{ESD})$ are the power spectra of $p_0(t)$ and $g(t,\text{ESD})$, respectively. The expected value of $S_m(f)$ with respect to the random times of arrival t_i is given by

$$< S_m(f) >= NS_0(f)S_g(f,\text{ESD}). \quad (3)$$

ESD estimates were obtained by minimizing the function [10]

$$\text{ESD} = \underset{\text{ESD}}{\arg\min}\sum_i \left(X(f_i,\text{ESD}) - \bar{X}\right)^2 \quad (4)$$
$$X(f) = 10\log\left(\hat{S}(f)/S_g(f,\text{ESD})\right),$$

where $\hat{S}(f)$ is the magnitude of $< S_m(f) >$ after compensating for the transducer impulse response and acoustic attenuation and $\bar{X}$ is the mean value of $X(f)$ within the analysis bandwith. Frequency-dependent acoustic attenuation effects were taken into account by using point attenuation compensation [10].

A box limited by the length of the window gate and the number of adjacent scan lines was termed the region of interest (ROI). The variance of $< S_m(f) >$, and therefore the variance of the QUS estimates, can be reduced if larger ROIs are used at the expense of spatial resolution, which results in typical ROI sizes that are much larger than the resolution cell of the imaging aparatus. The use of full angular spatial compounding allows multiple estimates per ROI that can be averaged in order to obtain more precise QUS images without sacrificing spatial resolution. A schematic of the proposed configuration is shown in Fig. 1.

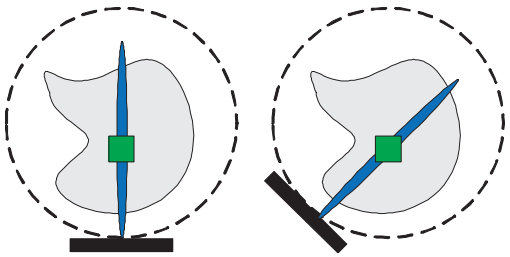

Fig. 1. Configuration for using compounding with QUS. The aperture (black rectangle) is rotated around the imaging target (irregular shape) over a full circular trajectory. The figure shows an ROI (green square) illuminated at 0° (left) and 45° (right).

B. WBU scanner description

A schematic of the WBU scanner is shown in Fig. 2. The scanner consists of a circular water tank where the breast of the patient is submerged for proper acoustic impedance coupling. The scanner can provide data in both transmission and reflection mode using several imaging arrays. All arrays are mechanically rotated describing a full circle of radius

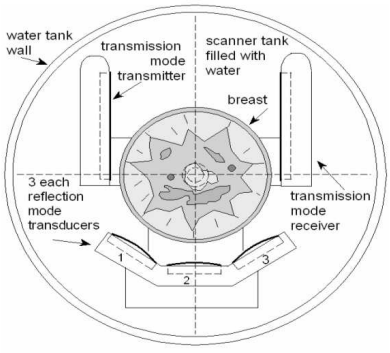

Fig. 2. Schematic of the WBU acoustic tomography scanner showing the locations of the transmission and reflection arrays.

approximately equal to 10 cm in order to obtain full angular coverage of the imaged breast.

The transmission mode data are acquired with two arrays (labeled as "transmission mode transmitter" and "transmission mode receiver" in Fig. 2) facing one another at opposite sides of the tank and operating at a nominal center frequency of 1 MHz. These data were used for constructing tomographic images of speed of sound. The reflection mode data are acquired with three arrays (labeled as 1, 2, and 3 in Fig. 2(a)) at approximately 45°, 90°, and 135° from the transmission mode transmitter array. The reflection mode arrays have 192 elements and operate at a nominal center frequency of 6 MHz. Several arrays are used so that their partially overlapping focal regions cover the space between the border of the tank and the center of rotation of the arrays. Therefore, an effective angular coverage of 180° can be obtained with the WBU scanner on reflection mode. The rf data collected by reflection array 1 were used in this study to reconstruct ESD images.

C. Experimental phantom and collected dataset

An experimental phantom was constructed in order to obtain preliminary experimental results using the WBU scanner. The phantom consisted of a gelatin cylinder with circular cross-section of 7.8 cm diameter and embedded A-glass 2429 beads (Potters Industries Inc., Valley Forge, PA) with mean diameter of 85 μm. The density, longitudinal sound speed, and Poisson ratio of the spheres used for the phantom preparation were 2.38 g/cm^3, 5.57 mm/μs, and 0.21, respectively. Using through-transmission with single-element 5 MHz transducers, the speed of sound and attenuation of the phantom were measured to be 1.61 mm/μs and 0.36 dB/cm/MHz, respectively. The $S_g(f,\text{ESD})$ function corresponding to a solid sphere embedded in fluid media was predicted using the theory developed by Faran [11] and later corrected by Hickling [12].

Tomographic images of speed of sound were obtained using inverse scattering algorithms [13]. An example is shown in Fig. 3(a). The speed of sound image exhibited an excellent agreement with the geometry and mean speed of sound contrast of the phantom. Some minor ringing artifacts and a hot spot at the center of the image were present due to slight calibration errors. The raw rf reflection-mode data was collected at 17

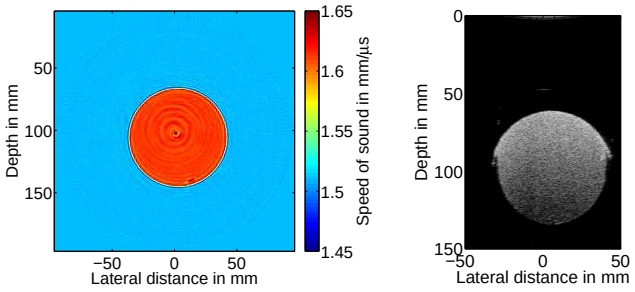

Fig. 3. (a) Inverse scattering image of speed of sound corresponding to the gelatin phantom. (b) B-mode image collected using the reflection-mode array of an ultrasonic tomography scanner.

angles of view between 0 and $360°$. A sample reflection mode image is shown in Fig. 3(b).

D. Data registration

In order to use angular compounding and QUS, the reflection-mode datasets needed to be registered. All datasets were registered relative to the speed of sound tomogram. It has been extensively documented that wavefronts are refracted (i.e., change their direction of propagation) when propagating in inhomogeneous media. If the wavelength can be considered small compared to the size of the scatterer, as in the case of the phantom used in this study, the wavefront refraction can be described using geometrical acoustics theory. In this work, the ray paths were calculated using the finite difference scheme presented in [14]. The refraction-corrected paths were used for the registration of QUS images obtained from the reflection-mode data.

III. Results

For all angles of view, the shape of the phantom in the reflection-mode images did not match the one in the acoustic tomogram as shown in the first row of Fig. 4. The refraction-corrected B-mode images are shown in the second row of Fig. 4. When using refraction correction, the correlation between the B-mode images and the acoustic tomogram was significantly improved and distortions were virtually eliminated.

The QUS estimates were obtained using ROIs of size 4 mm $\times$ 4 mm with a 50% overlap and the -9 dB bandwidth of the reflection-mode arrays. Only data from the surface of the array to the center of the tomography gantry were analyzed for each angle of view, which resulted in 17/2 = 8.5 effective angles of view per ROI. The average mean and standard deviation of the single angle-of-view estimates considering the 17 data sets were 85.4 μm and 12.2 μm, respectively. Sample QUS images obtained using data at four different angles of view are shown in Fig. 5.

A first compounded QUS image was obtained by averaging the single angle of view ESD estimates from all registered ROIs and is shown in Fig. 6(a). The resulting ESD mean and standard deviation of the compounded image were 85.4 μm and 4.7 μm, respectively. This constitutes an improvement in the standard deviation of the estimates by a factor of 2.6 when compared to the single angle of view case, which is in good agreement but slightly less than the theoretical expected value of approximately 2.9 ($\sqrt{8.5}$). The availability of several estimates per ROI, however, allows for more elaborate compounding techniques. As an example, a second compounded image was obtained by compounding the single angle of view estimates after discarding the most significant outlier when

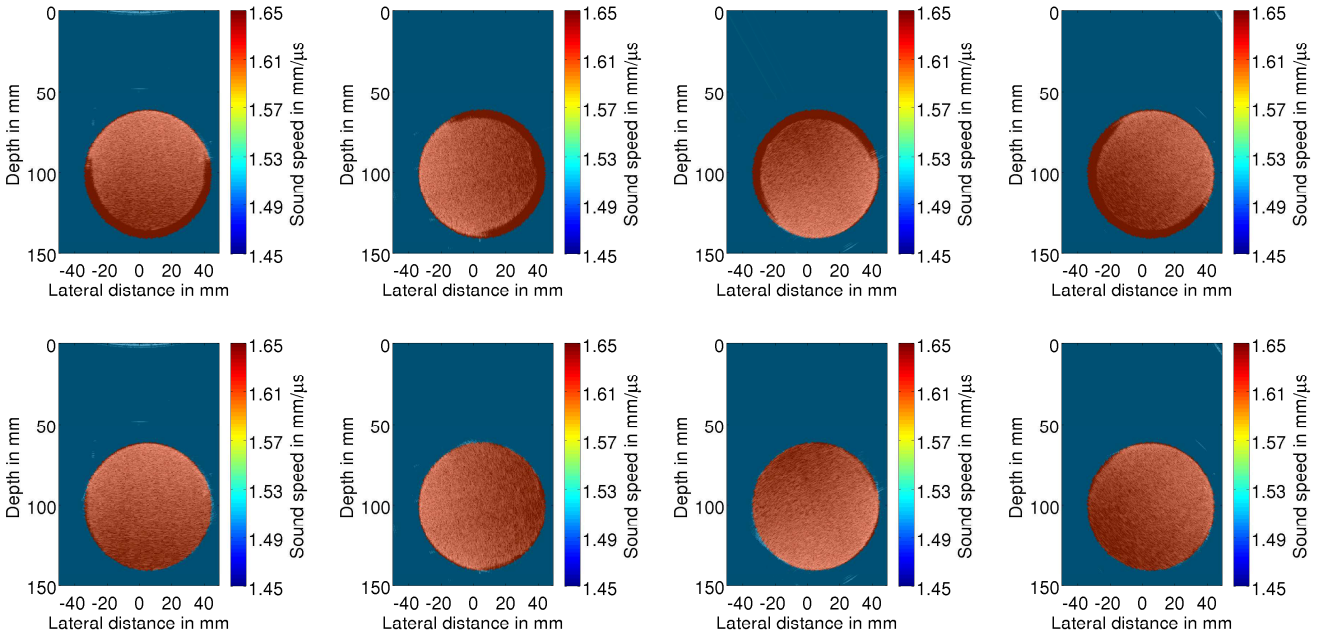

Fig. 4. Registered B-mode images collected using the reflection-mode array of an ultrasonic tomography scanner at four different angles of view. The speed of sound image is overlaid on top of the corresponding B-mode images both without (top) and with (bottom) refraction correction.

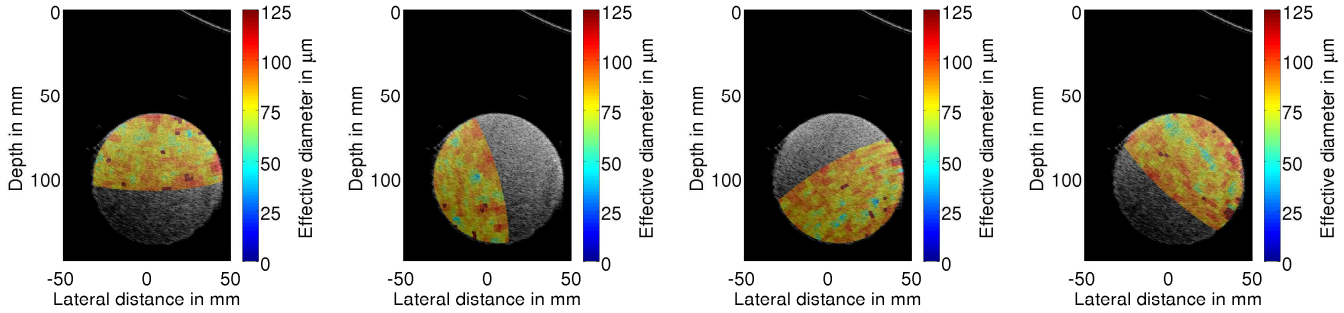

Fig. 5. ESD parametric images overlaid on top of the corresponding refraction-corrected B-mode images at four different angles of view.

compared to the median ESD estimate per pixel (see Fig. 6(b)). The resulting ESD mean and standard deviation of the compounded image were 85.2 μm and 4.1 μm, respectively. The improvement in standard deviation using the second compounding method by a factor of 3 outperformed the simpler compounding scheme and illustrates the potential advantages of obtaining several estimates per ROI.

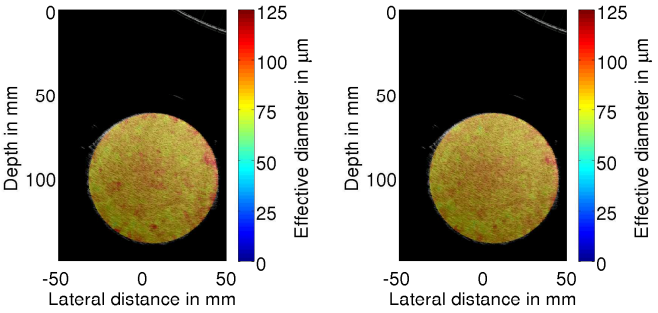

Fig. 6. ESD estimates obtained using the WBU acoustic tomography scanner and compounding. (a) ESD estimates obtained with full angular compounding using data at all angles of view. (b) ESD estimates obtained with full angular spatial compounding after discarding the most significant outlier per ROI.

IV. Conclusions

Previous studies [8] suggested that the use of full angular compounding significantly improves the trade off between spatial resolution in QUS imaging and precision of QUS estimates. The preliminary experimental results presented in this work represent the first implementation of QUS on an ultrasonic breast tomography scanner and demonstrate some of the benefits of integrating these technologies, i.e., the availability of full angular spatial compounding and integration with tomographic speed of sound images. The speed of sound images were used to correct for refraction and a novel compounding technique was implemented exploiting the fact that enough estimates per ROI were available to omit outliers. These methods find direct applicability for breast tissue characterization, for which full angular coverage is available.

V. Acknowledgements

The authors would like to thank Dr. James Wiskin, Dr. David Borup, Dr. Michael Insana, Dr. William D. O'Brien, Jr., and Kerry Hall. This work was funded by a grant from the National Institutes of Health (R43 CA121521).

References

[1] F.L. Lizzi, D.L. King, M.C. Rorke, J. Hui, M. Ostromogilsky, M.M. Yaremko, E.J. Feleppa, and P. Wai, "Comparison of theoretical scattering results and ultrasonic data from clinical liver examinations," *Ultrasound in Medicine and Biology*, vol. 14, no. 5, pp. 377–385, 1988.

[2] E.J. Feleppa, F.L. Lizzi, D.J. Coleman, and M.M. Yaremko, "Diagnostic spectrum analysis in ophthalmology: a physical perspective," *Ultrasound in Medicine and Biology*, vol. 12, no. 8, pp. 621–631, August 1986.

[3] M.F. Insana, T.J. Hall, and J.L. Fishback, "Identifying acoustic scattering sources in normal renal parenchyma from the anisotropy in acoustic properties," *Ultrasound in Medicine and Biology*, vol. 17, no. 6, pp. 613–626, 1991.

[4] E.J. Feleppa, A. Kalisz, J.B. Sokil-Melgar, F.L. Lizzi, T. Liu, A.L. Rosado, M.C. Shao, W.R. Fair, Y. Wang; M.S. Cookson, V.E. Reuter, and W.D.W Heston, "Typing of prostate tissue by ultrasonic spectrum analysis," *IEEE Transactions on Ultrasonics, Ferroelectrics, and Frequency Control*, vol. 43, no. 4, pp. 609–619, July 1996.

[5] M.L. Oelze, W.D. OBrien, Jr., J.P. Blue, and J.F. Zachary, "Differentiation and characterization of rat mammary fibroadenomas and 4T1 mouse carcinomas using quantitative ultrasound imaging," *IEEE Transactions on Medical Imaging*, vol. 23, no. 6, pp. 764–771, June 2004.

[6] A.L. Gerig, T. Varghese, and J.A. Zagzebsky, "Improved parametric imaging of scatterer size estimates using angular compounding," *IEEE Transactions on Ultrasonics, Ferroelectrics, and Frequency Control*, vol. 51, no. 6, pp. 708–715, June 2004.

[7] A.L. Gerig, Q. Chen, J.A. Zagzebsky, and T. Varghese, "Correlation of ultrasonic scatterer size estimates for the statistical analysis and optimization of angular compounding," *Journal of the Acoustical Society of America*, vol. 116, no. 3, pp. 1832–1841, September 2004.

[8] R. J. Lavarello, J. R. Sanchez, and M. L. Oelze, "Improving the quality of QUS imaging using full angular spatial compounding," in *IEEE Ultrasonics Symposium*, 2008, pp. 32–35.

[9] S. A. Johnson, T. Abbott, R. Bell, M. Berggren, D. Borup, D. Robinson, J. Wiskin, S. Olsen, and B. Hanover, "Noninvasive breast tissue characterization using ultrasound speed and attenuation," in *Acoustical Imaging*, vol. 28, 2007, pp. 147–154.

[10] M.F. Insana, R.F. Wagner, D.G. Brown, and T.J. Hall, "Describing small-scale structure in random media using pulse-echo ultrasound," *Journal of the Acoustical Society of America*, vol. 87, no. 1, pp. 179–192, January 1990.

[11] J. J. Faran, Jr., "Sound scattering by solid cylinders and spheres," *Journal of the Acoustical Society of America*, vol. 23, no. 4, pp. 405–418, July 1951.

[12] R. Hickling, "Analysis of echoes from a solid elastic sphere in water," *Journal of the Acoustical Society of America*, vol. 34, no. 10, pp. 1582–1562, October 1962.

[13] J. Wiskin, D. Borup, S. Johnson, M. Berggren, T. Abbott, and R. Hanover, "Full wave, non-linear, inverse scattering," in *Acoustical Imaging*, vol. 28, 2007, pp. 183–194.

[14] A. H. Andersen and A. C. Kak, "Digital ray tracing in two-dimensional refractive fields," *Journal of the Acoustical Society of America*, vol. 34, no. 10, pp. 1582–1562, October 1982.